CMNE/CILAMCE 2007
Porto, 13-15 Junho, 2007

NUMERICAL SIMULATION OF THE NONLINEAR BEHAVIOR OF RC BEAMS STRENGTHENED WITH NSM CFRP STRIPS

J. Sena Cruz[1]*, Joaquim Barros[1], Álvaro Azevedo[2] and A. Ventura Gouveia[3]

1: Civil Engineering Department
School of Engineering
University of Minho
Campus de Azurém, 4800-058 Guimarães, PORTUGAL
e-mail: jsena@civil.uminho.pt, barros@civil.uminho.pt web:http://www.civil.uminho.pt/composites/

2: Civil Engineering Department
Faculty of Engineering
University of Porto
Rua Dr. Roberto Frias, s/n 4200-465 Porto, PORTUGAL
e-mail: alvaro@fe.up.pt web: http://www.fe.up.pt/~alvaro

3: Civil Engineering Department
School of Technology
Polytechnic Institute of Viseu
Campus de Repeses, 3504-510 Viseu, PORTUGAL
e-mail: ventura@dcivil.estv.ipv.pt web: http://www.dcivil.estv.ipv.pt/dep/dcivil/

Keywords: Near Surface Mounted Reinforcement, Reinforced Concrete Beams, Strengthening, Carbon Fiber Reinforced Polymer Strips, Numerical Modeling.

Summary. *This paper describes some experimental tests carried out in the context of the evaluation of the bond behavior associated with NSM CFRP reinforcement. These results were used in the numerical simulation of the material nonlinear behavior of RC beams strengthened with NSM strips. For this purpose, an elasto-plastic multi-fixed smeared crack model was developed and implemented in the FEMIX computer code. The obtained numerical results are compared with those recorded in the experimental tests.*

1. INTRODUCTION

Strengthening structures with near surface mounted (NSM) carbon fiber reinforced polymer (CFRP) strips is a new technique that consists in the installation of CFRP strips into slits opened on the concrete cover. The strips are bonded to the concrete using an epoxy adhesive.
The preliminary experimental research carried out by Blaschko and Zilch in 1999 was based on the flexural strengthening of concrete structures with the NSM technique. Similar strengthening techniques were investigated by other researchers [1][2][3][4][5][6][7][8][9], which have shown the advantages of this technology. The application of the NSM technique to the shear strengthening of concrete structural elements has also been successfully investigated [2][10][11][12][13][14][15].
The experimental, analytical and numerical research carried out worldwide in the structural strengthening with composite materials is providing the knowledge that is being used by technical committees and task groups in the development of design recommendations [15][16][17][18]. However, only the CIDAR document [17] treats with detail the NSM technique. The ACI 440 and fib TG 9.3 committees have only recently assumed the purpose of treating the NSM technique with enough detail in order to produce well supported information to be included in their next official publications. According to these committees, the bond behavior between CFRP strips and concrete is one of the topics that requires more research, since it provides decisive information to be used in the development of analytical and numerical models.
In the present work a resume of the most relevant research carried out by the Composite Research Group [19] is presented. This research ranges from the experimental strip to concrete bond behavior to the numerical modeling of concrete structures strengthened with the NSM technique. The new constitutive models were implemented in a computer code that was developed by the authors of the present work [20], and whose purpose is the material nonlinear analysis of concrete structures.

2. BOND BEHAVIOR BETWEEN NSM CFRP STRIPS AND CONCRETE

In the context of this work, the word bond means the transfer of stresses between concrete and reinforcement in order to develop the composite action of both materials, during the loading process of reinforced concrete elements. Bond performance influences the ultimate load carrying capacity of a reinforced element, as well as some serviceability aspects, such as crack width and crack spacing. To assess the influence of bond length and load history on the bond performance, an experimental program was carried out. In the present section, the experimental research as well as the analytical modeling is briefly presented.

2.1. Pullout tests

Figure 1 shows the pullout bending test setup adopted in this study. Concrete blocks A and B are connected by a steel hinge located at mid-span close to the top, and by the CFRP fixed at the bottom. The bond test region was located in block A, with the bond length, L_b, being one of the variables to be studied. To ensure negligible slip of the strip fixed to block B and to

force bond failure in block A, the strip was bonded over a considerable length in block B. The slit made for the insertion of the CFRP was 15 mm deep and 4.8 mm wide.

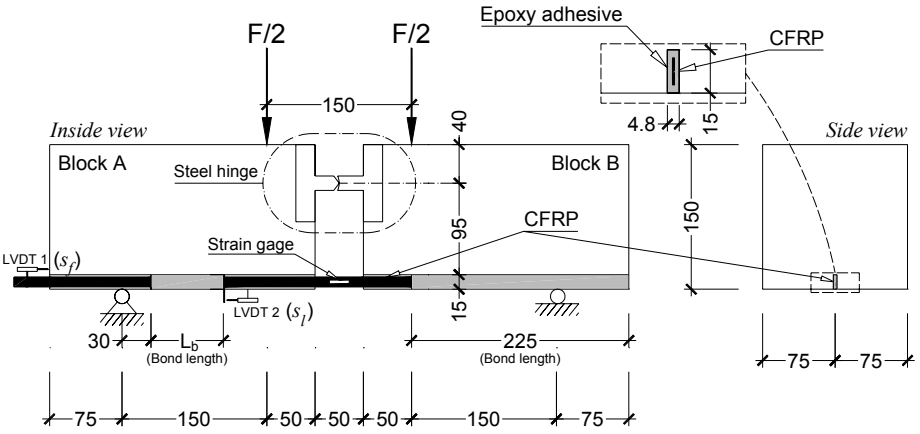

Figure 1. Setup of the pullout bending tests. Note: all dimensions are in millimeters.

The displacement transducer LVDT2 was used to control the test, at a constant 5 μm/s slip rate, and also to measure the slip at the loaded end, s_l, while the transducer LVDT1 was used to measure the slip at the free end, s_f. The strain gauge glued to the CFRP at the mid-span of the specimen was used to estimate the pullout force of the strip. A load cell mounted on the actuator was used to measure the total applied force, F. Further details describing the characteristics of the test setup can be found in [22].

The influence of the loading history on the bond performance associated with the NSM strengthening technique was treated in the present study by considering the following three types of load configurations: monotonic loading (M), one cycle of unloading/reloading at different slip levels (C1) and ten cycles of unloading/reloading for a fixed load level (C10). A total of seven series of tests composed the experimental program, each consisting of tests on three specimens. The generic denomination of each series is LbX_Y, where X is the CFRP bond length in millimeters (60, 90 or 120 mm), and Y is the type of load configuration (M, C1 or C10). Three distinct C10 load configurations were adopted, whose denominations are: Lb60_C10 series, Lb90_C10 series and Lb120_C10 series. In these series, the load level at the onset of the unloading/reloading cycles was 90%, 60% and 75% of the peak pullout force, respectively. In the C1 load configuration, one unloading/reloading cycle was performed at a loaded end slip of 250 μm, 500 μm, 750 μm, 1000 μm, 1500 μm, 2000 μm, 3000 μm and 4000 μm. All the tests were performed under displacement control at a rate of 5 μm/s, with the exception of the unloading phases of the cyclic tests, which were performed under load control with a predetermined load rate that corresponds to an average slip rate of 5 μm/s.

Material characterization includes the determination of the main properties of concrete, epoxy adhesive and CFRP strips. An average concrete compressive strength of 41.0±0.9 MPa was obtained at the age of the pullout bending tests. The CFRP strips had a thickness of 1.4 mm and a width of 10.0 mm. From five uniaxial tensile tests carried out according to the

ISO 527-5 [23] recommendations, the following properties were obtained: Young's modulus of elasticity equal to 171±1 GPa, tensile strength equal to 2.83±0.16 GPa, and ultimate strain equal to 1.55±0.10 %. To characterize the epoxy adhesive three-point bending tests and compression tests, following NP-EN 196-1 [24] recommendations, were carried out. From the performed bending tests, a tensile strength of 21.8±5.5 MPa was obtained. A compressive strength of 67.5±3.6 MPa was measured from the performed compression tests. Further details related to the material characterization can be found in [20].

In all the tested specimens the most significant failure occurred at the CFRP-adhesive interface. This was to be expected since the rougher surface of the concrete leads to a better bonding with the adhesive. Consequently, there is larger slip at the CFRP-adhesive interface during failure. Moreover, fine cracks in a fishbone pattern were observed in the epoxy adhesive.

Figure 2 shows typical relationships between the pullout force and the slip, at both the free and loaded ends (F_l-s_f and F_l-s_l), for the monotonic load configuration. These curves show that the relationship between the slip and the pullout force is nonlinear with the peak loads occurring at loaded end slips of 0.27 mm to 1.24 mm. After a sharp post-peak drop, the pullout force slowly decreases with an increase in the slip. The residual pullout forces, which are significant, indicate that frictional mechanisms in the CFRP-adhesive-concrete interfaces are mobilized during the pullout failure.

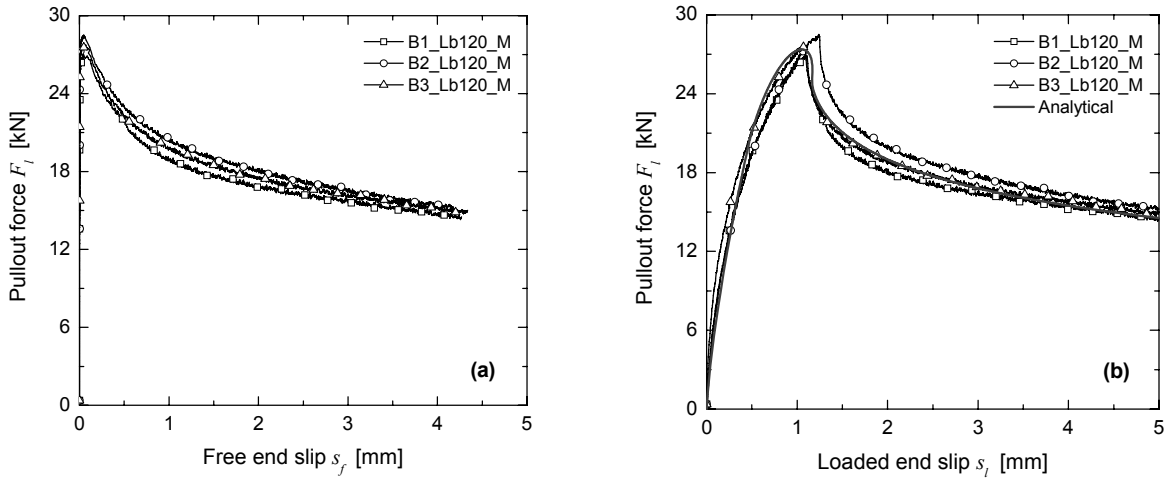

Figure 2. Relationships between pullout force and (a) free end and (b) loaded end slips for the Lb120_M series.

Based on the results of the monotonic tests, the following conclusions can be obtained [22]: the peak pullout force increases with L_b; the average bond strength, obtained by dividing the peak pullout force by the contact area between the CFRP and epoxy adhesive, ranges from 10 MPa to 14 MPa, with a tendency to decrease with the increase of L_b; the maximum tensile stress in the CFRP strip and the loaded end slip at peak pullout force increase with L_b.

Figure 3 shows the typical relationships between the pullout force and the slip at the free and loaded ends (F_l-s_f and F_l-s_l) for the C10 series. The complete test data of this series can be

found in [20]. The corresponding monotonic curve (Lb120_M) is also included in this figure. The curves of the C10 series are similar in shape to that of the corresponding monotonic test.

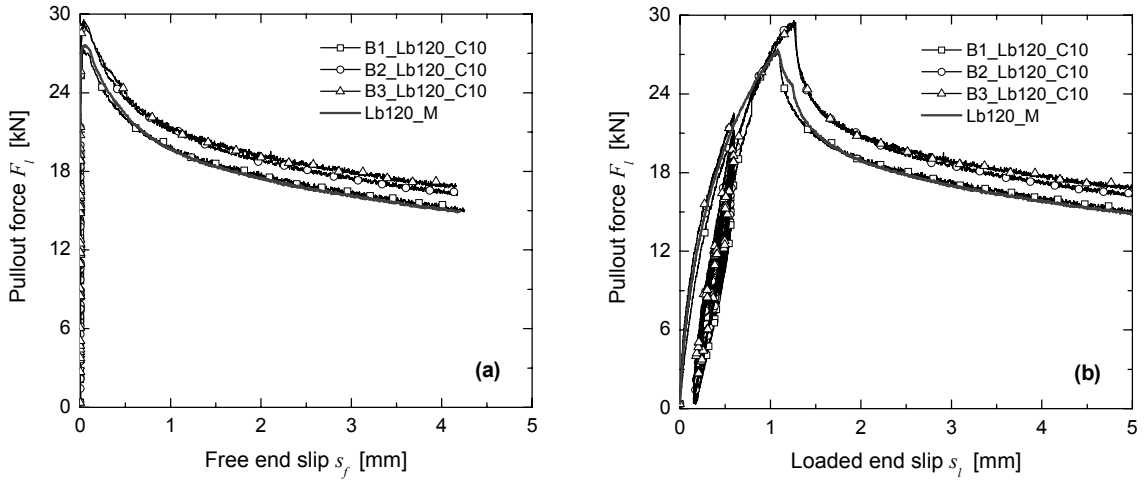

Figure 3. Relationships between pullout force and (a) free end and (b) loaded end slips for the Lb120_C10 series.

The results of the unloading/reloading tests with a fixed load level lead to the following conclusions [22]: the pullout force *versus* slip relationships in the cyclic tests (C10 series) and the curve obtained in the corresponding monotonic tests have a similar shape; in the unloading/reloading cycles a decrease of the pullout force at the end of the reloading branches, carried out before the peak pullout force, was observed; and the peak pullout force was not influenced by the cyclic loading.

For the C1 series, the relationships between the pullout force and the slip at the free and loaded ends (F_l-s_f and F_l-s_l) are shown in Figure 4, along with the corresponding monotonic curve. As expected, the curves of the cyclic tests have a shape that is similar to the monotonic curve. The free end slip remains constant during the unloading and reloading phases, indicating that the bond has not degraded along all its length. In the unloading/reloading tests at different slip levels, the stiffness decreases significantly up to the peak pullout force, after which there is a slight increase followed by a smooth decrease.

2.2. Analytical modeling

The following differential equation governs the slip of the CFRP bonded to concrete, as shown by Sena-Cruz and Barros [25]:

$$\frac{d^2 s}{dx^2} = \frac{2}{t_f E_f} \tau \tag{1}$$

where t_f and E_f are the thickness and the Young's modulus of the CFRP strip, respectively, s is the slip, i.e., the relative displacement between the CFRP and concrete, $\tau = \tau(s)$ is the local

bond stress-slip relationship within the length *dx*, and τ is the bond stress in the CFRP-adhesive interface. Eq. (1) is only valid when the following assumptions hold:

- the CFRP strip exhibits a linear elastic behavior in the longitudinal direction;
- the deformation of the concrete and adhesive is neglected.

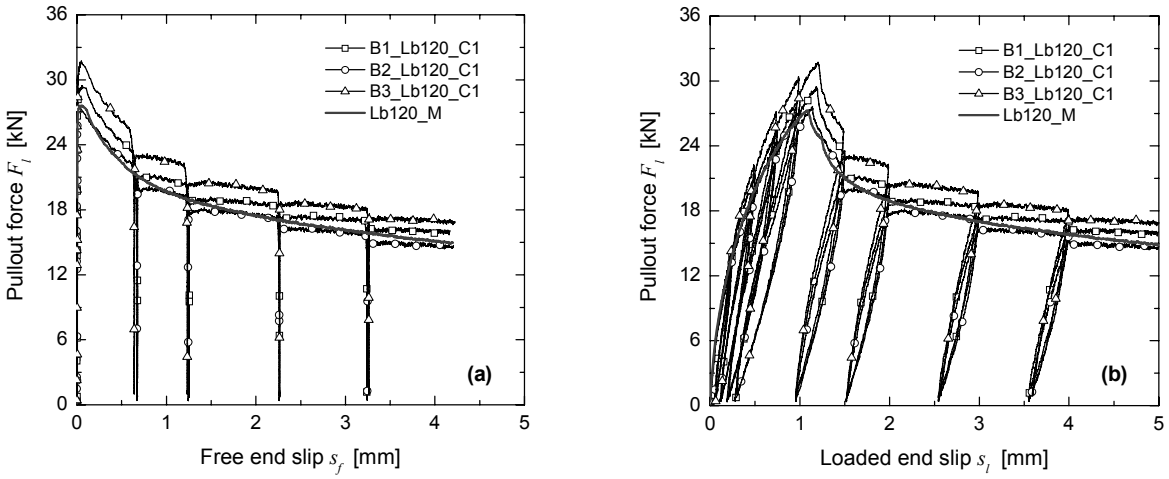

Figure 4. Relationships between pullout force and (a) free end and (b) loaded end slips for the Lb120_C1 series.

In the present work, the local bond stress-slip relationship is defined by the following functions,

$$\tau(s) = \tau_m \left(\frac{s}{s_m} \right)^{\alpha}, \ if \ \ s \le s_m \tag{2}$$

$$\tau(s) = \tau_m \frac{1}{1 + \left(\frac{s - s_m}{s_1} \right)^{\alpha'}}, \ if \ \ s > s_m \tag{3}$$

In these equations, τ_m and s_m are the bond strength and the corresponding slip, respectively, and α, α' and s_1 are the parameters that define the shape of the corresponding curve.
A numerical strategy was developed [25], using the loaded end slip and the pullout force values obtained in the pullout-bending tests described in the previous section. This approach yields the values of the parameters s_m, τ_m, α, α' and s_1 of Eqs. (2) and (3) by solving Eq. (1). The distribution of the slip and the bond stress along the bond length is taken into account.
Figure 2(b) shows, for one of the tests in the monotonic series, that the analytically obtained pullout force *versus* loaded end slip relationship fits the corresponding experimental results satisfactorily. Similar results have been obtained for the other monotonic series (see [20]).

3. NUMERICAL ANALYSIS

A series of beams strengthened with the NSM technique were tested up to failure. The corresponding results are described later in this paper. These tests were simulated with a numerical tool, developed by the authors, and termed FEMIX 4.0. The main characteristics of this computer code are described in the following section.

3.1. Software for nonlinear material analysis

FEMIX 4.0 is a computer code whose purpose is the analysis of structures by the Finite Element Method (FEM). This code is based on the displacement method, being a large library of types of finite elements already available, namely 3D frames and trusses, plane stress elements, flat or curved elements for shells, and 3D solid elements. Linear elements may have two or three nodes, plane stress and shell elements may be 4, 8 or 9-noded and 8 or 20 noded hexahedra may be used in 3D solid analyses. This element library is complemented with a set of point, line and surface springs that model elastic contact with the supports, and also a few types of interface elements to model inter-element contact. Embedded line elements can be added to other types of elements to model reinforcement bars. All these types of elements can be simultaneously included in the same analysis, with the exception of some incompatible combinations. The analysis may be static or dynamic and the material behavior may be linear or nonlinear. Data input is facilitated by the possibility of importing CAD models. Post processing is performed with a general purpose scientific visualization program named *drawmesh*.
In the same nonlinear analysis several nonlinear models may be simultaneously considered, allowing, for instance, the combination of reinforced concrete with strengthening components, which exhibit distinct nonlinear constitutive laws. Interface elements with appropriate friction laws and nonlinear springs may also be simultaneously considered. The global response history is recorded in all the sampling points for selected post-processing.
Advanced numerical techniques are available, such as the Newton-Raphson method combined with arc-length techniques and path dependent or independent algorithms. When the size of the systems of linear equations is very large, a preconditioned conjugate gradient method can be advantageously used.

3.2. Elasto-plastic multi-fixed smeared crack model

In this section, a brief description of the elasto-plastic multi-fixed smeared crack model implemented in the FEMIX computer code is presented. More details can be found elsewhere [22]. In the present model, after the occurrence of a crack and/or plastic strain in a sampling point, the total incremental strain is decomposed in a crack strain, an elastic reversible strain and an irreversible or plastic strain. The crack strain is governed by the fracture parameters of the material, while the strain between cracks is used in an elasto-plastic material model.
Two different yield surfaces were used: the Rankine criterion for concrete under traction and the Owen & Figueiras [26] yield surface for the concrete under compression. An isotropic

hardening rule was adopted in the elasto-plastic model, with a strain hardening flow rule. The assumed hardening/softening diagram can be found elsewhere [22].
The behavior of the cracked concrete is governed by the multi-fixed smeared crack model. In each sampling point several non-orthogonal cracks can arise. The crack evolution in fracture mode I can be simulated using a tri-linear tension softening or stiffening diagram (see Figure 5(a)). The fracture mode II is simulated using the shear retention factor. In the present numerical model the crack band-width can be estimated in three different ways: equal to the square root of the area of the finite element, equal to the square root of the area of the integration point or equal to a constant value.

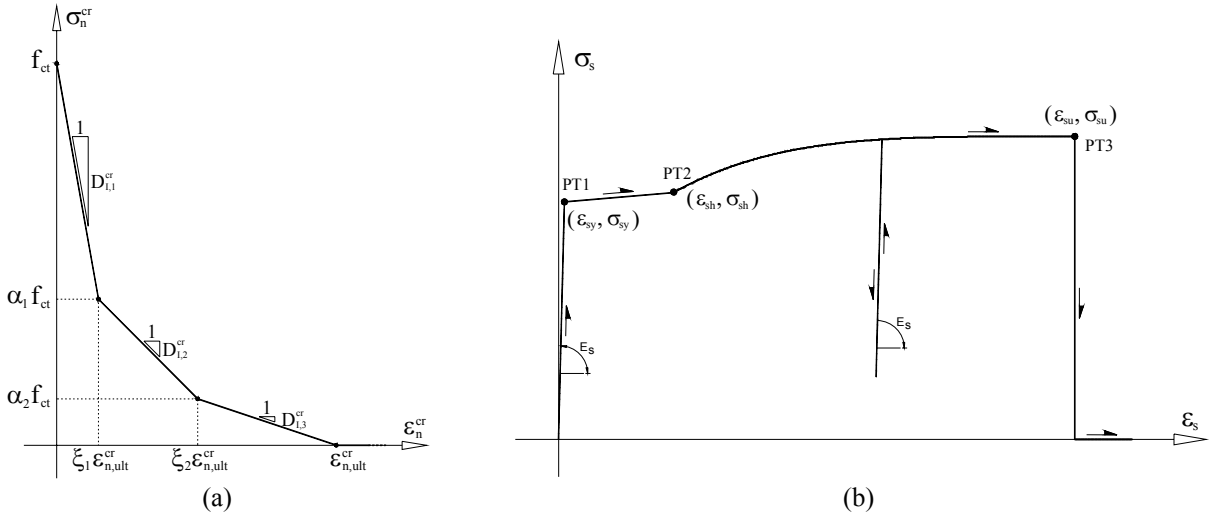

Figure 5. (a) Tension softening or stiffening diagram. (b) Uniaxial constitutive model of the rebars.

The equilibrium equations involved in the constitutive material model leads to a system of nonlinear equations. This system is solved using the Newton-Raphson method. The developed model includes implicit Euler backward algorithms and consistent tangent operators.

3.3. Uniaxial constitutive model of the reinforcement

Figure 5(b) represents the adopted uniaxial constitutive model of the rebars. The curve (under compressive or tensile loading) is composed of four branches (see equation (4)). To define the four branches, three points PT1=(ε_{sy},σ_{sy}), PT2=(ε_{sh},σ_{sh}) and PT3=(ε_{su},σ_{su}) and the parameter p are required. Typically, the value of the parameter p varies between 1.0 and 4.0. Further details can be found elsewhere [20].

$$\sigma(s)=\begin{cases} E_s\varepsilon_s & if\ \varepsilon_s \le \varepsilon_{sy} \\ E_{sy}\left(\varepsilon_s-\varepsilon_{sh}\right)+\sigma_{sh} & if\ \varepsilon_{sy} < \varepsilon_s \le \varepsilon_{sh} \\ \sigma_{su}+\left(\sigma_{sh}-\sigma_{su}\right)\left(\dfrac{\varepsilon_{su}-\varepsilon_s}{\varepsilon_{su}-\varepsilon_{sh}}\right)^p & if\ \varepsilon_{sh} < \varepsilon_s \le \varepsilon_{su} \\ 0 & if\ \varepsilon_s > \varepsilon_{su} \end{cases} \quad (4)$$

3.4. Modeling of beams with flexural strengthening

In this section the simulation of the experimental tests carried out by Barros and Fortes [4] is presented. The main purpose of this experimental program was to assess the ability of the NSM strengthening technique as a means of increasing the flexural capacity of reinforced concrete beams. Two distinct analyses are performed: in the former a perfect bond between the CFRP and concrete is assumed, while in the latter slip can occur.

Figure 6 to Figure 8 show the geometry, finite element mesh, loading configuration and support conditions adopted in this study. The reference beams (V1, V2, V3 and V4) are simulated with the setup shown in Figure 6, whereas Figure 7 and Figure 8 present the setup adopted for the strengthened beams (V1R1, V2R2, V3R2 and V4R3) assuming perfect bond and allowing slip at the CFRP-concrete interface, respectively. The height of each beam can be found elsewhere [4]. To simulate the concrete part of the specimen, 8-node Serendipity plane stress elements with 3×3 Gauss-Legendre integration scheme were used. The longitudinal and transverse steel reinforcements, as well as the CFRP strips, were simulated with 3-node quadratic embedded cable elements with two Gauss-Legendre integration points. When slip is allowed at the CFRP-concrete interface, the CFRP strips are simulated with 3-node quadratic cable elements with two Gauss-Legendre integration points, and the CFRP-concrete interface is discretized with 6-node quadratic interface elements with two Gauss-Lobatto integration points.

Table 1 includes the concrete properties used in the numerical simulations. From the mean value of the experimentally obtained compressive strengths, f_{cm}, all the other parameters were estimated [20]. To simulate the post-cracking behavior of reinforced concrete, a tri-linear tension-stiffening diagram is used. The material that exhibits this type of behavior is located in the first rows of each finite element mesh, counting from the bottom of the beam. In the parts of the mesh where no longitudinal reinforcement is present (upper rows), a tri-linear tension-softening diagram is used. In the cases where CFRP reinforcement is also present, the post-cracking behavior of concrete must be treated differently. Therefore, a realistic tension-stiffening model for the simulation of the post-cracking behavior of these elements should also take into account the properties of the CFRP materials. In the present work, the tri-linear stress-strain diagram, represented in Figure 5(a), is used to simulate the post-cracking behavior of reinforced concrete elements strengthened with CFRP materials. The main advantage of this diagram is the possibility of changing the values of ξ_1, α_1, ξ_2 and α_2, thus providing enough flexibility in order to model the most important aspects of the

tension-stiffening effect.

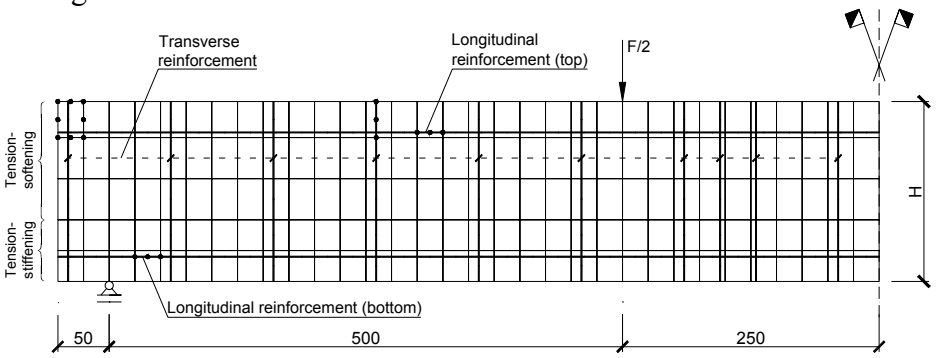

Figure 6. Geometry, mesh, loading and support conditions of reinforced concrete beams. Note: all dimensions are in millimeters.

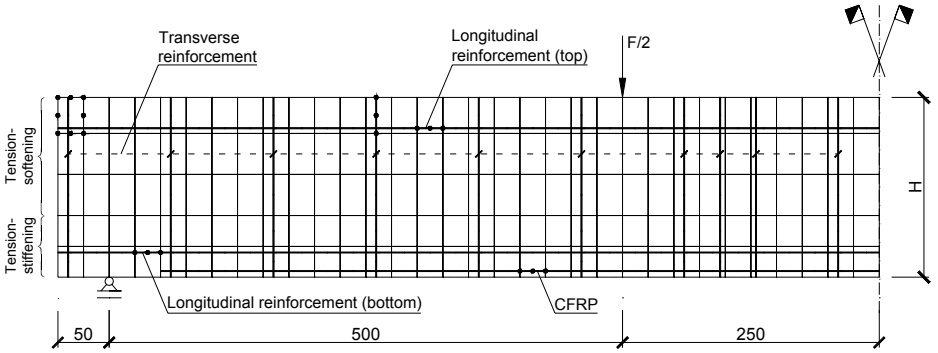

Figure 7. Geometry, mesh, loading and support conditions of reinforced concrete beams strengthened with CFRP strips. Perfect bond between the CFRP and concrete is assumed. Note: all dimensions are in millimeters.

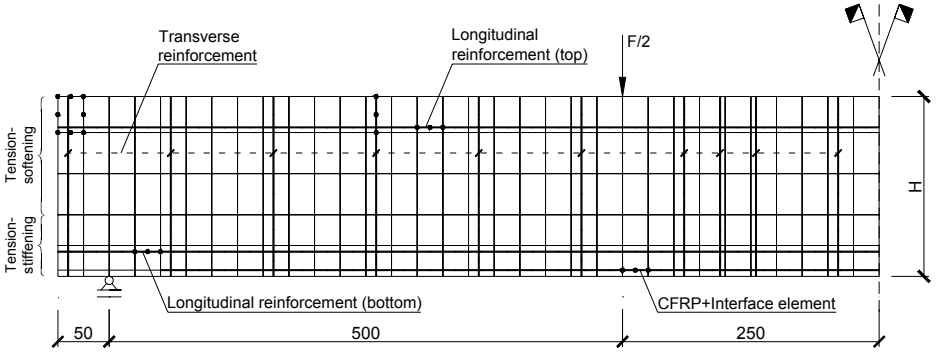

Figure 8. Geometry, mesh, loading and support conditions of reinforced concrete beams strengthened with CFRP strips. Bond-slip at the CFRP-concrete interface is modeled. Note: all dimensions are in millimeters.

Poisson's ratio	$\nu_c = 0.15$
Initial Young's modulus	$E_c = 35757$ N/mm^2
Compressive strength	$f_c = 46.0$ N/mm^2
Strain at peak compression stress	$\varepsilon_{c1} = 2.2\times10^{-3}$
Parameter defining the initial yield surface	$\alpha_0 = 0.3$
Tri-linear tension-softening diagram	$f_{ct} = 3.0$ N/mm^2 ; $G_f = 0.087$ N/mm $\xi_1 = 0.02$; $\alpha_1 = 1/3$; $\xi_2 = 0.48$; $\alpha_2 = 1/6$
Tri-linear tension-stiffening diagram of the beams V1, V2, V3 and V4	$f_{ct} = 3.0$ N/mm^2 ; $G_f = 0.24$ N/mm $\xi_1 = 0.05$; $\alpha_1 = 0.5$; $\xi_2 = 0.8$; $\alpha_2 = 0.4$
Tri-linear tension-stiffening diagram of the beams V1R1, V2R2, V3R2 and V4R3	$f_{ct} = 3.0$ N/mm^2 ; $G_f = 0.7$ N/mm $\xi_1 = 0.1$; $\alpha_1 = 0.6$; $\xi_2 = 0.45$; $\alpha_2 = 0.3$
Shear retention factor	*Exponential* ($p_1 = 2$)
Parameter defining the mode I fracture energy available to the new crack	$p_2 = 2$
Crack band-width	*Square root of the area of the element*
Threshold angle	$\alpha_{th} = 60^o$

Table 1. Concrete properties used in the simulation of beams with flexural strengthening.

All the parameters that define the material model of the rebars (longitudinal and transverse reinforcements) and CFRP strips are included in Table 2. These parameters were estimated by Barros and Fortes [4].

Reinforcement	$(\varepsilon_{sy};\sigma_{sy})$	$(\varepsilon_{sh};\sigma_{sh})$	$(\varepsilon_{su};\sigma_{su})$	p
∅3	$(8.97\times10^{-4};175)$	$(1.44\times10^{-1};288)$	$(1.44\times10^{-1};288)$	1.0
∅6	$(3.50\times10^{-3};700)$	$(5.00\times10^{-3};760)$	$(3.17\times10^{-2};800)$	1.0
∅8	$(2.62\times10^{-3};524)$	$(3.00\times10^{-2};554)$	$(1.50\times10^{-1};614)$	2.6
CFRP	$(17.1\times10^{-3};2700)$	$(17.1\times10^{-3};2700)$	$(17.1\times10^{-3};2700)$	1.0

Table 2. Concrete properties used in the simulation of beams with flexural strengthening. Note: all stresses are in megapascal.

In the present numerical analysis the following relationship is adopted to simulate the nonlinear behavior of the CFRP-concrete interface

$$\tau(s)=\begin{cases}16\left(\dfrac{s}{0.3}\right)^{0.2} & if \;\; s\le 0.3\ \text{mm}\\ 16\left(\dfrac{s}{0.3}\right)^{-0.3} & if \;\; s>0.3\ \text{mm}\end{cases} \tag{5}$$

In all the numerical simulations the load is applied by direct displacement-control at the loaded point.

Figure 9 and Figure 10 show the relationship between deflection at beam mid-span and load, for both the experimental tests and the numerical analyses (assuming perfect bond). The main aspects observed in the experimental tests of the reference beams (V1, V2, V3 and V4), such as crack initiation, stiffness degradation, yield initiation of the rebars, and load carrying capacity are well simulated. The exception occurred in beam V3, where the model has predicted a crack initiation load greater than the experimentally observed one. A possible reason for this discrepancy is a slight damage of beam V3 that might have occurred before the test. Due to some difficulties in the convergence of the Newton-Raphson iterative procedure, the predicted ultimate deflection was lower than the one obtained experimentally in the reference beams.

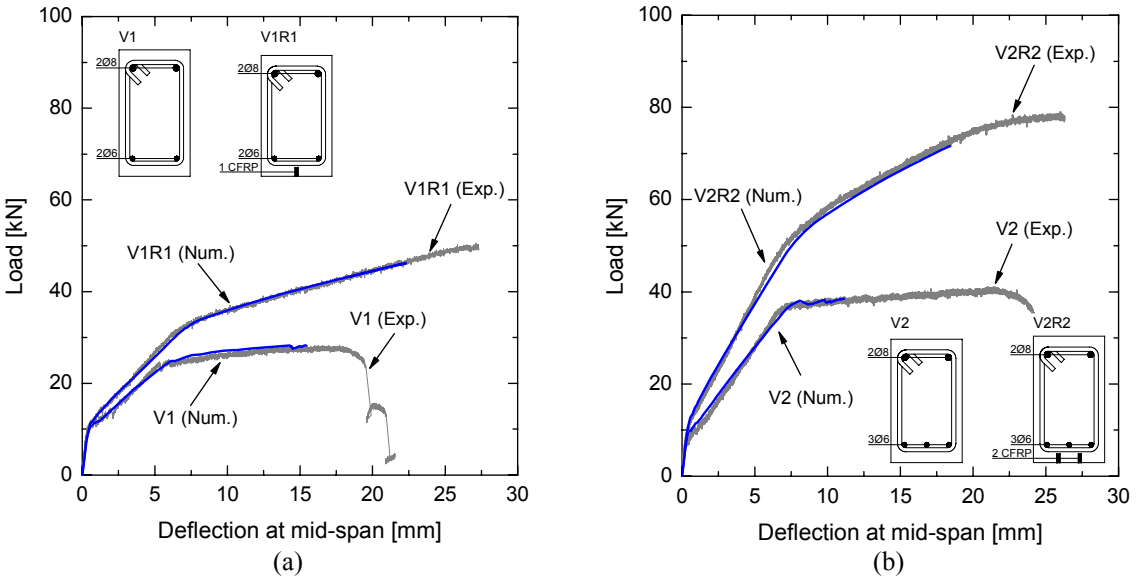

Figure 9. (a) Load *vs.* deflection at mid-span obtained experimentally and numerically (assuming perfect bond) for the beams: (a) V1 and V1R1; (b) V2 and V2R2.

The numerical simulation of the strengthened beams (V1R1, V2R2, V3R2 and V4R3), assuming perfect bond at the CFRP-concrete interface, has also reproduced the main aspects observed in the experimental tests. However, the numerical model did not predict the maximum load carrying capacity obtained experimentally, due to the non-convergence of the Newton-Raphson iterative procedure at a load level of about 90% of the experimental

maximum load carrying capacity. For all the strengthened beams, the maximum difference between the numerically obtained ultimate load and the experimentally observed maximum load did not exceed 12 % of the latter.
Modeling the bond-slip behavior at the CFRP-concrete interface did not contribute to an increase of the maximum deflection obtained in the analyses with perfect bond, thus indicating that in this type of beams the slip between the CFRP and concrete has a marginal contribution to the global response.

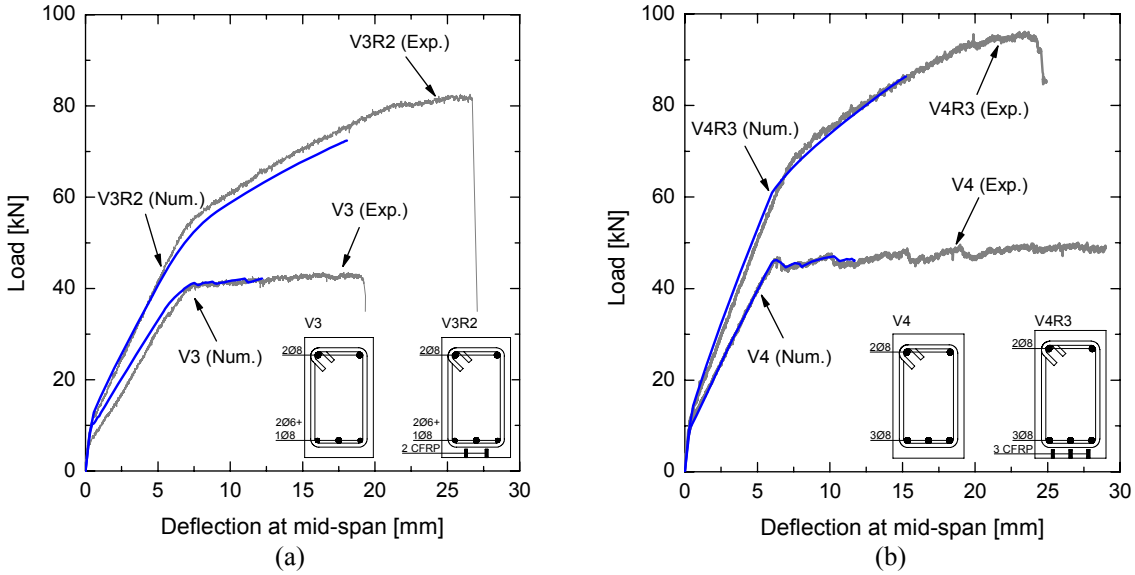

Figure 10. (a) Load *vs.* deflection at mid-span obtained experimentally and numerically (assuming perfect bond) for the beams: (a) V3 and V3R2; (b) V4 and V4R3.

3.5. Modeling of shear strengthened beams

The performance of the NSM technique as a means of increasing the shear strength of reinforced concrete beams was experimentally assessed by Barros and Dias [12], being the beams composing the VA series selected for the numerical simulation described below.
Figure 11 and Figure 12 show the geometry, finite element mesh, loading configuration and support conditions adopted in this study. To simulate the concrete part of the specimen, 8-node Serendipity plane stress elements with 3×3 Gauss-Legendre integration scheme are used. The longitudinal and transverse steel reinforcements, as well as the CFRP strips, are simulated with 3-node quadratic embedded cable elements with two Gauss-Legendre integration points. The assumption of perfect bond between the reinforcement and concrete is adopted.

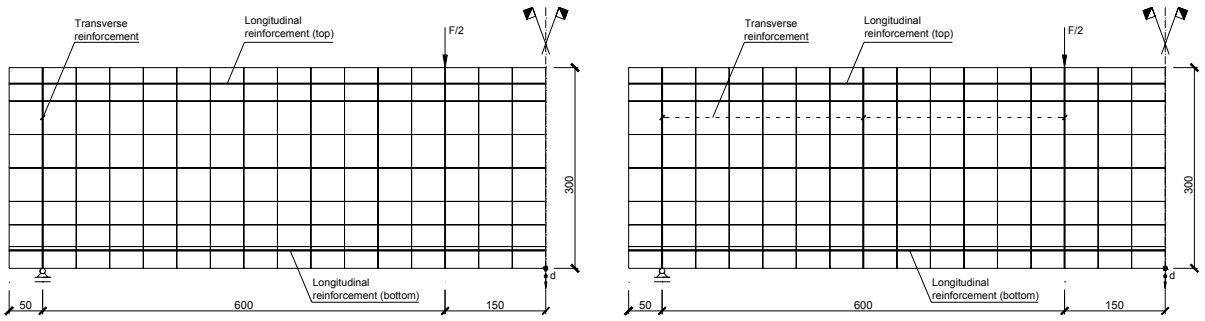

(a) (b)

Figure 11. Geometry, mesh, loading configuration and support conditions of beams VA10 (a) and VAE-30 (b). Note: all dimensions are in millimeters.

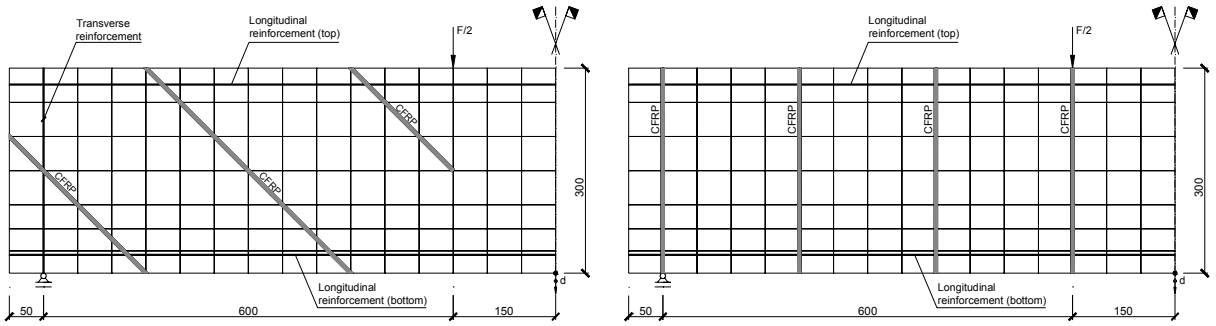

(a) (b)

Figure 12. Geometry, mesh, loading configuration and support conditions of beams VACI-30 (a) and VACV-20 (b). Note: all dimensions are in millimeters.

The concrete properties adopted in the present analyses are included in Table 3. In this table the experimentally obtained value of the compressive strength, f_{cm} is indicated. All the other parameters depend on the mean value of f_{cm}. Since the longitudinal steel reinforcement ratio is high, the effect of the tension-stiffening is negligible. For this reason the post-cracking behavior of concrete is simulated with a tri-linear tension-softening diagram. Two distinct numerical analyses are performed for the beams VAE-30, VACI-30 and VACV-20, considering two values of the threshold angle, 30º or 60º.

Table 4 includes the properties of the rebars and CFRP reinforcements. In all the numerical simulations the load is applied by direct displacement-control at the point located in the lower right corner of the mesh.

Figure 13 and Figure 14 show the relationship between the load and the deflection at mid-span, for both the experimental test and the numerical simulations. For the beams VAE-30, VACI-30 and VACV-20, the numerical simulations with values of the threshold angle equal to 30º and 60º are included in these figures.

In the beam VA10, a good agreement between the numerical and experimental results is

obtained. The crack initiation, the ultimate load and the beam deformability are well predicted.

Poisson's ratio	$\nu_c = 0.15$
Initial Young's modulus	$E_c = 36567$ N/mm^2
Compressive strength	$f_c = 49.2$ N/mm^2
Strain at peak compression stress	$\varepsilon_{c1} = 2.2\times10^{-3}$
Parameter defining the initial yield surface	$\alpha_0 = 0.3$
Tri-linear tension-softening diagram	$f_{ct} = 3.0$ N/mm^2 ; $G_f = 0.09$ N/mm $\xi_1 = 0.1$; $\alpha_1 = 0.5$; $\xi_2 = 0.3$; $\alpha_2 = 0.2$
Shear retention factor	*Linear* ($p_1 = 1$)
Parameter defining the mode I fracture energy available to the new crack	$p_2 = 0.5$
Crack band-width	*Square root of the area of the element*
Threshold angle	$\alpha_{th} = 30^o$ or $\alpha_{th} = 60^o$

Table 3. Concrete properties used in the simulation of shear strengthened beams.

Reinforcement	$(\varepsilon_{sy};\sigma_{sy})$	$(\varepsilon_{sh};\sigma_{sh})$	$(\varepsilon_{su};\sigma_{su})$	p
∅6 (Transverse reinforcement)	$(2.70\times10^{-3};540)$	$(1.0;540)$	$(1.0;540)$	1.0
∅6 (Longitudinal reinforcement)	$(3.11\times10^{-3};622)$	$(1.0;622)$	$(1.0;622)$	1.0
∅10	$(3.00\times10^{-3};600)$	$(1.0;600)$	$(1.0;600)$	1.0
CFRP	$(14.7\times10^{-3};2200)$	$(14.7\times10^{-3};2200)$	$(14.7\times10^{-3};2200)$	1.0

Table 4. Reinforcement properties used in the simulation of shear strengthened beams. Note: all stresses are in megapascal.

Figure 15 shows the numerical crack pattern at the last converged combination of the beam VA10. In this figure only the cracks with the *opening* and *fully open* statuses are represented. The experimental crack pattern at impending failure of the beam VA10 is depicted in Figure 16. It can be observed that the beam failed by shear due to the occurrence of large deformations in the main shear crack indicated in the figure. This crack is well predicted by the numerical model, since a well defined shear crack band is formed in a location that

coincides with the observed experimental shear crack and has the same orientation. In this shear crack band several cracks have a *fully open* status. However, numerical convergence is too difficult to obtain at this stage, since several cracks are forming and, simultaneously, existing cracks are changing their status.

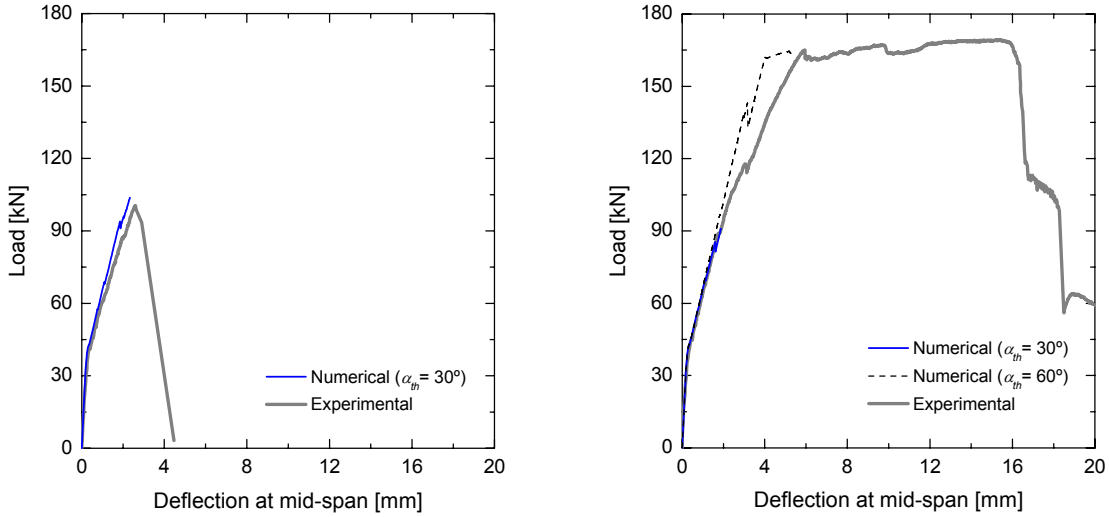

Figure 13. Load *vs.* deflection at mid-span obtained experimentally and numerically for the beams VA10 (a) and VAE-30 (b).

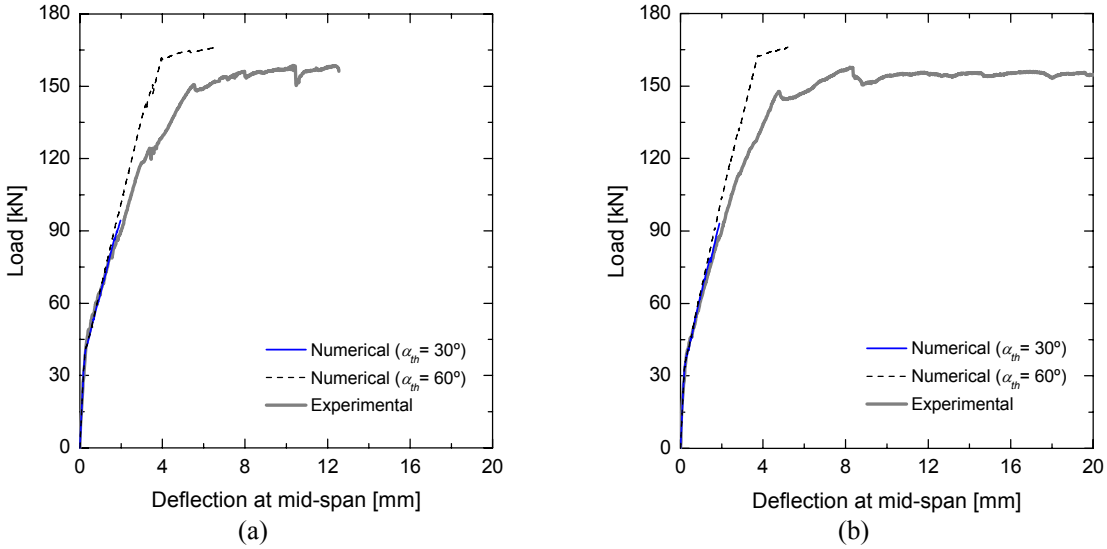

Figure 14. Load *vs.* deflection at mid-span obtained experimentally and numerically for the beams VACV-20 (a) and VACI-30 (b).

When a 30º threshold angle is adopted, the numerical simulation of the beam VAE-30, which has transverse reinforcement, did not converge for a load level close to the failure load of the

beam VA10, which has no transverse reinforcement. For the available numerical results, the relationship between the load and the deflection at mid-span accurately fits the experimental data as shown in Figure 13(b). When a 30º threshold angle is considered, the Newton-Raphson algorithm does not converge in an intermediate combination that corresponds to the evolution of the shear crack band. This non-convergence is due to the formation of several cracks and to the simultaneous occurrence of a significant number of critical crack status changes in the existing cracks.

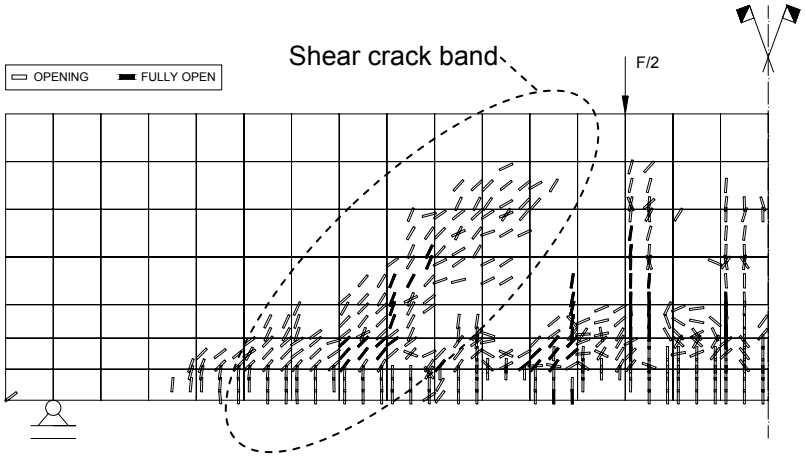

Figure 15. Numerical crack pattern of the beam VA10 at the last converged combination.

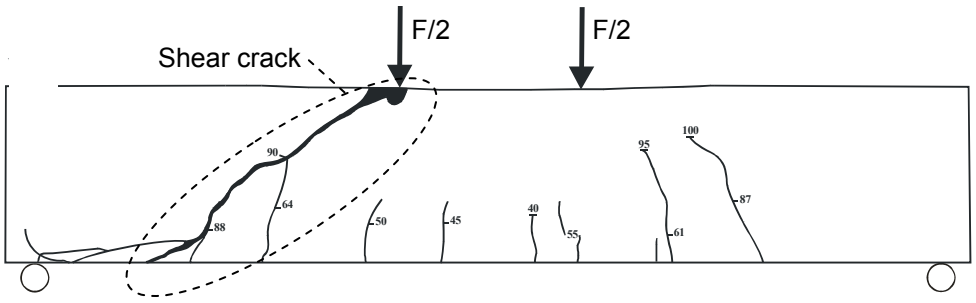

Figure 16. Experimental crack pattern of the beam VA10 at impending failure [12].

Figure 13(b) also includes the numerical analysis with a 60º threshold angle. In this analysis, a new crack can only be formed when the principal stress exceeds the concrete tensile strength and the angle between the direction of the existing cracks and the direction of the principal stress exceeds 60º. For this reason the response is stiffer than the one experimentally observed and stiffer than the numerical response with a 30º threshold angle. In the analysis with a 60º threshold angle, the stress in the longitudinal reinforcement reaches the yield stress, in agreement with the experiments. However, the numerical crack pattern does not accurately match the experimental crack pattern. In fact, in the numerical model, all cracks in *fully open* status are located in the pure bending zone and the shear crack band is formed closer to the support of beam.

The results of the numerical simulations performed with the VACI-30 and VACV-20 beams are similar to those described for the beam VAE-30. Similar numerical difficulties were encountered in the simulations performed with a 30º threshold angle.

4. CONCLUSIONS

In the present work the experimental characterization of the bond behavior between NSM CFRP strips and concrete is described. In this experimental program the influence of the bond length and loading configuration on the bond behavior was studied. From the obtained results the following main conclusions can be pointed out: the pullout force increases when the bond length increases and the monotonic tests correspond to the envelope of the cyclic tests. Using a numerical strategy a local bond stress-slip relationship was assessed.

A nonlinear material model was developed to numerically simulate RC beams strengthened with the NSM technique. Flexural and shear strengthened beams were analyzed. The developed elasto-plastic multi-fixed smeared crack model was implemented in the FEMIX computer code. Two distinct analyses were performed: in the former a perfect bond between the CFRP and concrete was assumed, while in the latter slip could occur. From the numerically obtained results the following conclusions arise: the main aspects observed in the experimental tests were reproduced by the numerical model, namely crack initiation, stiffness degradation, yield initiation of the rebars, and load carrying capacity; modeling the bond-slip behavior at the CFRP-concrete interface did not contribute to more accurate solutions; the adoption of a small value for the threshold angle leads to some instabilities in the numerical simulation.

REFERENCES

[1] Blaschko, M. and Zilch, K. *Rehabilitation of concrete structures with CFRP strips glued into slits*. *International. Conference on Composite Materials*, Paris, (1999), pp. 7.

[2] Carolin, A. “Carbon fibre reinforced polymers for strengthening of structural elements.” *PhD thesis*, Division of Structural Engineering, Luleå University of Technology, Sweden, (2003), pp. 190.

[3] El-Hacha, R. and Rizkalla, S. H. “Near surface mounted FRP reinforcements for flexural strengthening of concrete structures.” *ACI Struct. J.*, Vol. **101**, No. 5, pp. 717-726, (2004).

[4] Barros, J.A.O. and Fortes, A.S. “Flexural strengthening of concrete beams with CFRP laminates bonded into slits.” *Journal Cement and Concrete Composites*, Vol. **27**, No. 4, pp. 471-480, (2005).

[5] Kotynia, R. *Strengthening of reinforced concrete structures with near surface mounted FRP reinforcement*. *5th International Conference - Analytical Models and New Concepts in Concrete and Masonry Structures AMCM 2005*, Gliwice - Ustroń, (2005), pp. 8.

[6] Jung, W.T., Park, Y.H., Park, J.S, Kang, J.Y, and You, Y.J. *Experimental investigation on flexural behavior of RC beams strengthened by NSM CFRP reinforcements*. *7th Int. Symposium, Fiber-Reinforced (FRP) Polymer Reinforcement for Concrete Structures -*

FRPRCS-7, C.K. Shield, J.P. Busel, S.L. Walkup, and D.D. Gremel eds., American Concrete Institute, Farmington Hills, Mich, (2005), pp. 795-806.

[7] Barros, J.A.O., Ferreira, D.R.S.M., Fortes, A.S., and Dias, S.J.E. "Assessing the effectiveness of embedding CFRP laminates in the near surface for structural strengthening." *Construction and Building Materials Journal*, Vol. **20**, pp. 478-491, (2006).

[8] Liu, I.S.T., Oehlers, D.J., and Seracino, R. "Tests on the ductility of reinforced concrete beams retrofitted with FRP and steel near-surface mounted plates." *J. Compos. Constr.*, Vol. **10**, No. 2, pp. 106-114, (2006).

[9] Bonaldo, E., Barros, J.A.O., and Lourenço, P.B. "Efficient strengthening technique to increase the flexural resistance of existing RC slabs: NSM CFRP laminates and compressive thin bonded SFRC overlay." *Technical Report No. 09-DEC/E-06*, Department of Civil Engineering, University of Minho, (2006), pp. 118.

[10] De Lorenzis, L. and Nanni, A. "Shear strengthening of reinforced concrete beams with near-surface mounted fiber reinforced polymer rods." *ACI Struct. J.*, Vol. **98**, No. 1, pp. 60-68, (2001).

[11] Nanni, A., Di Ludovico, M. and Parretti, R. "Shear strengthening of a PC bridge girder with NSM CFRP rectangular bars." *Advances in Structural Engineering*, Vol. **7**, No. 4, pp. 97-109, (2004).

[12] Dias, S.J.E. and Barros, J.A.O. *NSM CFRP Laminates for the Shear Strengthening of T Section RC Beams*. *2nd International fib Congress***,** Naples**,** (2006), Paper ID 10-58**.**

[13] De Lorenzis, L. and Rizzo, A. *Behavior and capacity of RC beams strengthened in shear with NSM FRP reinforcement*. *2nd International fib Congress*, Naples, (2006), Paper ID 10-9.

[14] Barros, J.A.O. and Dias, S.J.E. "Near surface mounted CFRP laminates for shear strengthening of concrete beams." *Journal Cement and Concrete Composites*, Vol. **28**, No. 3, pp. 276-292, (2006).

[15] Fédération Internationale du Béton (FIB) *Externally bonded FRP reinforcement for RC structures*. Bulletin 14, Lausanne, Switzerland, (2001), pp. 138.

[16] ACI Committee 440. *Guide for the design and construction of externally bonded FRP systems for strengthening concrete structures*. American Concrete Institute, ACI Committee 440, (2002), pp. 118.

[17] Centre for Infrastructure Diagnosis, Assessment and Rehabilitation (CIDAR). *Design Guideline for RC structures retrofitted with FRP and metal plates: beams and slabs*. DRAFT 3, Submitted to Standards Australia 02/02/06, The University of Adelaide, (2006).

[18] CNR-DT 200. *Instructions for design, execution and control of strengthening intervention with FRP*. Consiglio Nazionale delle Richerche, Roma, Italy, (2006), pp. 144.

[19] http://www.civil.uminho.pt/composites

[20] Sena-Cruz, J.M. "Strengthening of concrete structures with near-surface mounted CFRP laminate strips." *PhD Thesis*, Department of Civil Engineering, University of

Minho, (2004).
<http://www.civil.uminho.pt/composites/Publications/2006/JA2006_004_JCCC.pdf>

[21] Azevedo A.F.M., Barros J.A.O., Sena-Cruz J.M. and Gouveia A.V. *Software no ensino e no projecto de estruturas (Educational software for the design of structures)*. *III Congresso de Luso-Moçambicano de Engenharia*, Maputo, Mozambique, (2003), pp. 81-92.
<http://civil.fe.up.pt/pub/people/alvaro/pdf/2003_Mocamb_Soft_Ens_Proj_Estrut.pdf>

[22] Sena-Cruz, J.M., Barros, J.A.O., Gettu, R. and Azevedo, F.M. "Bond behavior of near surface mounted CFRP laminate strips under monotonic and cyclic loading." *Journal of Composites for Construction*, Vol. **10**, No. 4, pp. 295-303, (2006).

[23] ISO 527-5 "Plastics – Determination of tensile properties – Part 5: Test conditions for unidirectional fibre-reinforced plastic composites." *International Organization for Standardization* (ISO), Geneva, Switzerland, (1997).

[24] NP-EN 196-1 "Methods testing cements." *CEN*, Brussels, Belgium, (1987).

[25] Sena-Cruz, J.M., and Barros, J.A.O. "Modeling of bond between near-surface mounted CFRP laminate strips and concrete." *Computers & Structures*, ELSEVIER, Special issue: Computational Mechanics in Portugal, C. Mota Soares and J. Barbosa eds, 82/17-19, pp. 1513-1521, (2004).

[26] Owen, D.R.J. and Figueiras, J.A. "Anisotropic elasto-plastic finite element analysis of thick and thin plates and shells." *International Journal for Numerical Methods in Engineering*, Vol. **19**, p. 323-350, (1983).